Journal of Colloid and Interface Science 633 (2023) 886–896

Contents lists available at ScienceDirect

Journal of Colloid and Interface Science

journal homepage: www.elsevier.com/locate/jcis

Regulated electrochemical performance of manganese oxide cathode for potassium-ion batteries: A combined experimental and first-principles density functional theory (DFT) investigation

Bidhan Pandit [a,*], Sachin R. Rondiya [b,c], Shoyebmohamad F. Shaikh [d], Mohd Ubaidullah [d], Ricardo Amaral [e], Nelson Y. Dzade [b,e], Emad S. Goda [f,g], Abu ul Hassan Sarwar Rana [h], Harjot Singh Gill [i], Tokeer Ahmad [j]

[a] Department of Materials Science and Engineering and Chemical Engineering, Universidad Carlos III de Madrid, Avenida de la Universidad 30, 28911 Leganés, Madrid, Spain
[b] School of Chemistry, Cardiff University, Main Building, Park Place, Cardiff CF10 3AT, Wales, UK
[c] Department of Materials Engineering, Indian Institute of Science (IISc), Bengaluru 560012, Karnataka, India
[d] Department of Chemistry, College of Science, King Saud University, P.O. Box 2455, Riyadh 11451, Saudi Arabia
[e] Department of Energy and Mineral Engineering, Pennsylvania State University, University Park, PA 16802, United States
[f] Organic Nanomaterials Lab, Department of Chemistry, Hannam University, Daejeon 34054, Republic of Korea
[g] Fire Protection Laboratory, National Institute of Standards, 136, Giza 12211, Egypt
[h] Department of Electrical and Electronic Engineering, The University of Melbourne, Parkville VIC 3010, Australia
[i] University Centre for Research & Development, Mechanical Department, Chandigarh University, Gharuan, Mohali, Punjab, India
[j] Nanochemistry Laboratory, Department of Chemistry, Jamia Millia Islamia, New Delhi 110025, India

HIGHLIGHTS

- Development of α-MnO_2 nanorods as a cathode material for potassium-ion battery.
- The voltage window is optimized for the prepared cathode.
- α-MnO_2 exhibits first discharge capacity of 142 mAh/g and good rate performance.
- The intercalation of potassium into the MnO_2 matrix is studied using DFT studies.
- DFT studies show diffusion barrier of 0.31 eV for K^+ through 1D tunnel of α-MnO_2.

GRAPHICAL ABSTRACT

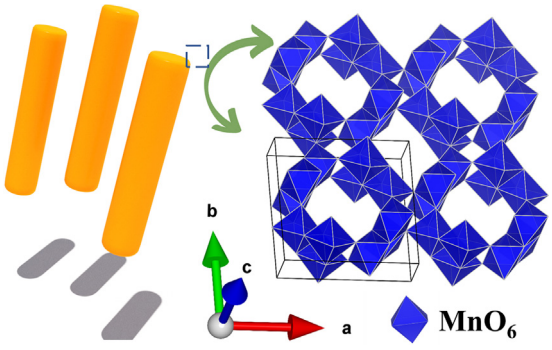

ARTICLE INFO

Article history:
Received 7 September 2022
Revised 8 November 2022
Accepted 12 November 2022
Available online 15 November 2022

Keywords:
Manganese oxide
Nanorods
Cathode
Potassium-ion battery
Density functional theory

ABSTRACT

Potassium-ion batteries (KIBs) are promising energy storage devices owing to their low cost, environmental-friendly, and excellent K^+ diffusion properties as a consequence of the small Stoke's radius. The evaluation of cathode materials for KIBs, which are perhaps the most favorable substitutes to lithium-ion batteries, is of exceptional importance. Manganese dioxide (α-MnO_2) is distinguished by its tunnel structures and plenty of electroactive sites, which can host cations without causing fundamental structural breakdown. As a result of the satisfactory redox kinetics and diffusion pathways of K^+ in the structure, α-MnO_2 nanorods cathode prepared through hydrothermal method, reversibly stores K^+ at a fast rate with a high capacity and stability. It has a first discharge capacity of 142 mAh/g at C/20, excellent rate execution up to 5C, and a long cycling performance with a demonstration of moderate capacity retention up to 100 cycles. X-ray diffraction (XRD), X-ray photoelectron spectroscopy (XPS), and density functional theory (DFT) simulations confirm that the K^+ intercalation/deintercalation occurs through 0.46 K movement between Mn^{IV}/Mn^{III} redox pairs. First-principles density functional theory (DFT)

* Corresponding author.
E-mail address: bpandit@ing.uc3m.es (B. Pandit).

https://doi.org/10.1016/j.jcis.2022.11.070

calculations predict a diffusion barrier of 0.31 eV for K^+ through the 1D tunnel of α-MnO_2 electrode, which is low enough to promote faster electrochemical kinetics. The nanorod structure of α-MnO_2 facilitates electron conductive connection and provides a strong electrode–electrolyte interface for the cathode, resulting in a very consistent and prevalent execution cathode material for KIBs.

1. Introduction

Rechargeable batteries as reasonable and practical energy storage systems that can integrate the major energy sources, such as wind and solar, into the electric grids are critical in today's energy-based society [1–3]. Among the various rechargeable ion batteries (Li [4–6], Na [7–14], Al [15–17], Mg [18–22] etc.), research groups have opted to move further with the investigation of potassium-ion batteries (KIBs) [23–29]. Potassium is the second most abundant base metal after sodium as well [30]. Furthermore, the KIB advancement can be achieved from the smallest potential for the K^+/K redox pair in various common organic electrolytes used for ion battery applications [31–38]. The practical as well as theoretical computations have revealed that the K^+/K (-2.88 V) redox couple can show the least reduction potential in ordinary solvents such as propylene carbonate (PC) [39,40]. This might guide towards a much broader voltage window, which would result in a high energy density for KIBs, as projected. Another advantage of KIBs is the fundamentally weaker Lewis acidity of K ion, resulting in small solvated ions. Furthermore, because K ions have a low desolvation energy, they may diffuse more quickly through the electrolyte/electrode interface in a coordinated pathway. Another advantageous feature is that potassium does not associate with any alloy formation it in contact with aluminum at relatively lower voltages, which corresponds to reduced cell production cost by replacing copper with an aluminum anode.

However, because this advancement is still in the planning stages, great foresight and planning advances are required to solve the existing issues. During the charge/discharge process, for example, the continuous insertion and extraction of K^+ with a greater radius of 0.138 nm will simply disrupt the structure of used cathode materials, achieving low capacity, reduced rate execution, poor stability, and even inactivity in electrochemical performance. Another disadvantage is that electrode materials which are relatively heavier are responsible for achieving low-energy density performance as well. Along these points, there is a crucial need to recognize first structural and electrochemical properties of various electrodes investigated for KIBs, and then develop electrochemically advantageous both cathode and anode materials, to manufacture full cell KIBs. There are reports on the KIBs, nevertheless, the total research articles in this field are still limited.

Carbonaceous materials [41], elementary substance materials (P [42], Sn [43], Sb [44]and Bi [45]), alloys (K-Na [46] and Sn_4P_3 [47]), organics [48], transition metal (TM) carbides [49], oxides [50] and sulfides [51] have all been confirmed as potential anodes for KIBs. Until now, only a few materials (for example, organics, polyanionic combinations, and Prussian blue analogues) have been studied as cathodes for KIBs, confirming the feasibility of reversible K^+ deintercalation/intercalation with sufficient mechanism studies. Furthermore, the development of TM oxides with a high reversible capacity and stable electrochemical mechanism are effectively emphasized as cathode materials for Li/Na-ion batteries, which also add new members to electrode category for KIBs.

Mn-based materials are supposed to be promising cathodes for rechargeable batteries due to their inexpensive, abundance and non-toxic qualities [52]. Because of their potential usage as cathode materials for Li/Na-ion batteries, Mn-based compounds have been extensively investigated [53]. In addition, Mn-containing electrode materials for K-ion insertion/extraction have gained a lot of interest [54]. Manganese dioxide (MnO_2), one of the Mn-containing oxides, has been extensively considered as one of a potential electrode materials because to its conventional benefits of high theoretical capacity, low cost and earth-abundance [55]. The crystal structure of MnO_2 can be broadly classified into three types based on the interlinking configurations of the octahedral MnO_6 building blocks: one-dimensional (1D) tunnel structures (α-MnO_2, β-MnO_2, and γ-MnO_2), two-dimensional (2D) layer structures (δ-MnO_2), and three-dimensional (3D) mesh structures (λ-MnO_2) [56]. The morphology, crystal structure, size, and surface area of those MnO_2 crystal structures directly influence the electrochemical properties [57]. Among the several structural polymorphs of MnO_2, the α-MnO_2 phase has structural advancement with a greater interlayer dissipation, which is important for cation diffusion. α-MnO_2 structure provides paths for particle intercalation and deintercalation because to its open structure. In the present study, we suggest a hydrothermal approach for preparing homogenous α-MnO_2 nanorods for high-performance KIBs. The nanorod structure creates a web network, which enhances conductivity and allows volume expansion in the active material as well. We show that KIB with a voltage window of 1–4 V have higher capacity and rate capability with near to 100 % Coulombic efficiency, which is much better than the KIB with a voltage window of 1.5–4 V. Electrochemical tests with a voltage window of 1–4 V reveal that MnO_2 has an extremely high K-storage capacity (primary discharge capacity of 142 mAh/g), a high rate capability (C/20 to 5C), and moderate cycling stability (up to 100 cycles). Because it combines high capacity and stability with the help of structural advancement, this electrode material is a superior cathode material for next-generation KIBs.

2. Experimental synthesis and techniques

2.1. α-MnO_2 preparation

In alkaline conditions, the oxidation of a manganese (II) acetate (98 %, Sigma-Aldrich) with ammonium persulfate (98 %, Sigma-Aldrich) results in MnO_2 preparation as illustrated in previously reported article [58] (Scheme 1). First and foremost, the desired sodium hydroxide (anhydrous, ≥98 %, Sigma-Aldrich) (100 ml) aqueous solution was prepared and divided into two parts: one for manganese acetate and the other for ammonium persulfate precursors. Then, the ammonium persulfate-containing mixture was progressively filled with the manganese-associated precursor to prepare a complex solution. This complex was placed in a Teflon lined hydrothermal autoclave and heated at 180 °C for 12 h. The resulting dispersion was washed with ethanol and water before drying for 12 h at 60 °C.

Two synthetic reactions are associated in our manganese dioxide preparation approach. Manganese hydroxide complex is acquired by the association of manganese acetate with sodium hydroxide the in the first step:

$$(CH_3COO)_2Mn + 3OH^- = Mn(OH)_3^- + 2CH_3COO^-. \quad (1)$$

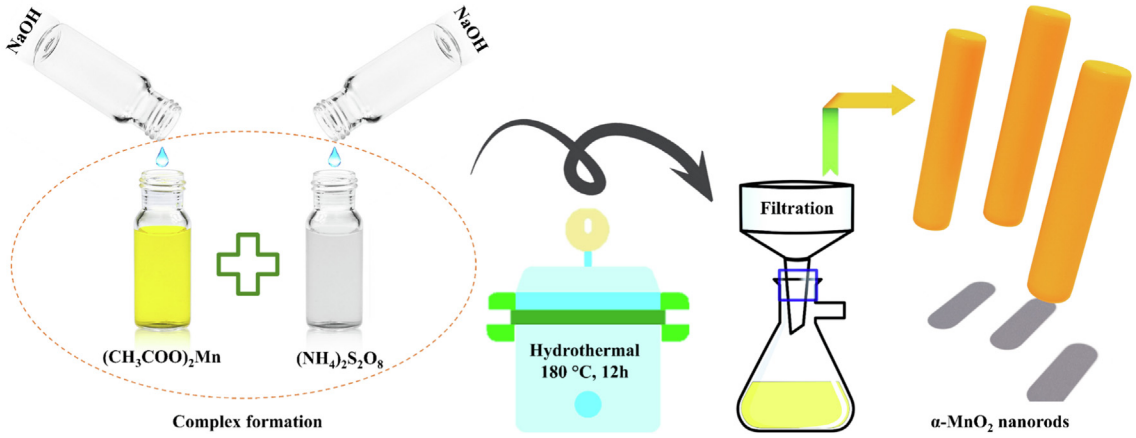

Scheme 1. Scheme of α-MnO_2 synthesis.

In association earlier condition, the next step includes an oxidoreduction reaction between manganese hydroxide and persulfate anions:

$$Mn(OH)_3^- + S_2O_8^{2-} + OH^- = MnO_2 + 2SO_4^{2-} + 2H_2O. \quad (2)$$

2.2. Characterizations

The Powder XRD analysis was carried out using a Bruker D8 Advance diffractometer (CuKα = 1.54056 nm), which confirmed the formation of high-quality powders of α-MnO_2. The Raman spectrum for the material was obtained using the Horiba LabRAM HR spectrometer, and the contrasting spectrum was recorded between 100 and 1000 cm^{-1}. The X-ray photoelectron spectroscopy (XPS) (ESCALAB 250 (ThermoElectron)) was examined using a monochromatic Al Kα radiation, hv = 1486.6 eV. The morphologies were studied using field emission scanning electron microscopy (FESEM) and high resolution transmission electron microscopy (HRTEM) captured by using Hitachi S-4800 and FEI TECNAI G2 20 Twin instruments, respectively.

The details coin cell fabrication with electrochemical parameters and DFT Computation are illustrated in **Supplementary Information, Section 1 and 2**.

3. Results and discussion

3.1. Structural and morphological analysis

Fig. 1**a** depicts the standard powder X-ray diffraction, ensuring the tetragonal structure of α-MnO_2 (space group *I*4/*m*) with the reference of JCPDS #44–141. The diffraction peaks at 12.7°, 18.1°, 25.6°, 28.7°, 37.5°, 41.9°, 49.7°, 55.9°, 60.0°, 65.1°, 69.1°, and 72.7° can be assigned to the crystallographic planes of 110, 200, 220, 310, 211, 301, 411, 600, 521, 002, 541, and 312, respectively. The tetragonal α-MnO_2 structure with edge and corner-sharing MnO_6 units, as shown in the inset of Fig. 1**b**, provides adequate space for efficient K^+ ions diffusion, which is necessary for excellent electrochemical performance. Among all the MnO_2 polymorphs, this α-MnO_2 tunnel structure is particularly interesting due to the typical 1D structure allowing ions for (de)intercalation in conjunction with the change of manganese oxidation states during redox reactions. The crystallite size is also supported from the structural analysis [59,60].

Meanwhile, the development of as-prepared α-MnO_2 was also analyzed by using the Raman spectrum for **Fig. S1**. It shows clear peaks detected at 179, 581, and 640 cm^{-1} allocated for as-synthesized material [61]. The intense peaks at 581 and 640 cm^{-1} are ascribed to the symmetric vibrations of the Mn-O and the modes that follow the interstitial space associated tetragonal α-MnO_2 structure. Furthermore, the peak at 179 cm^{-1} is due

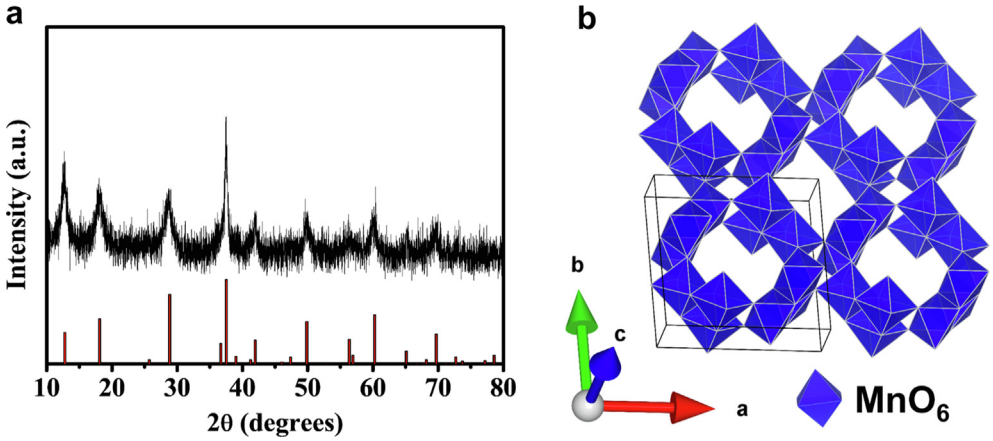

Fig. 1. (a) XRD spectrum of α-MnO_2. (b) Crystal structure.

to the MnO_6 octahedra related translational vibration for the ions into the tunnel structure [62].

However, XPS spectrum was engaged to examine the oxidation states of prepared α-MnO_2 (Fig. 2**a**). The NaOH precursor utilized in the synthesis of MnO_2 is mainly responsible for the existence of small Na KL1 and Na1 s peaks. The survey spectrum is consistent with earlier investigations [63–69]. Fig. 2**b, c** shows the standard core-level XPS spectra of associated Mn 2p and O1s. As shown in Fig. 2**b**, the Mn 2p spectrum is separated into doublet pointing at 642.5 and 654.2 eV, which are associated with 2p3/2 and 2p1/2, respectively. The binding difference between the above-mentioned doublet of Mn 2p is about 11.7 eV, implying the formation of Mn^{4+}. Overall, the O1 s core-level spectrum is presented in Fig. 2**c**, which depicts two distinct surface oxygen parts, one at 530 eV which corresponds to lattice oxygen and the other at 531.3 eV which associates with loosely coordinated or defected oxygen [70].

FESEM and HRTEM were used to study a comprehensive morphological and fundamental assessment of the α-MnO_2 nanorods. The FESEM photos of coordinated α-MnO_2 nanorods with homogeneous size are clearly demonstrated in Fig. 3**a, b**. The TEM image in Fig. 3**c, d** shows that the as-organized α-MnO_2 nanorods associate with a uniform diameter between 10 and 50 nm. This morphology further promotes electrical conductivity and more charge transport channels by virtue of the higher surface area, achieving a good electrode/electrolyte interface and small ion diffusion length [71–73]. The electron beam of the SEM was scanned across the sample along a predetermined line to detect X-rays at certain points along that line. An examination of the X-ray energy spectrum at each point show graph of the relative elemental concentration of each element as a function of position along the line. The data is represented qualitatively by the line scan profile that depicts the increase or decrease of all elemental elements present at all places along the line (Fig. 3**e**). The Mn and O signals exhibit a steady intensity pattern over the length of the nanorod, indicating a homogenous distribution of the associated components; nonetheless, the presence of Mn and O in a 1:2 ratio suggests the presence of pure MnO_2.

3.2. Electrochemical performance of α-MnO_2 electrode

Fig. 4 demonstrates the charge/discharge profiles and cycle execution of α-MnO_2 electrode (active electrode mass loading of 2–6 mg/cm^2) at different voltage windows in K cells linked to KPF_6 in ethylene carbonate (EC): Diethyl carbonate (DEC) electrolyte at current rate of C/20. As shown in Fig. 4**a, 0.18** potassium can be inserted into α-MnO_2 by utilizing a C/20 rate up to 1.5 V against K^+/K during the 1st discharge, out of which only 0.13 potassium can be extracted on the run of subsequent charge process, causing a moderate reversible capacity of 40 mAh/g. We changed the discharge voltage limit from 1.5 to 1 V and evaluated the electrochemical properties of α-MnO_2 at 1–4 V since it showed greater intercalation in this window (Fig. 4**c**). As a result, there is 0.46 potassiation, leading to the formation of $K_{0.46}MnO_2$. During the primary charge, an irreversibility of 0.2 K is predicted at the final voltage of 4 V. In present case, the α-MnO_2 electrode reaches a high capacity of 142 mAh/g for the primary discharge process, with a charge capacity of 81 mAh/g and Coulombic efficiency of 57 %, as illustrated in Fig. 4**d**. In the two cells, the associated charge and discharge characteristics are almost identical. Even in both cases, an irreversible limit is seen at the first cycle, which is determined to be due to significant electrolyte decomposition to form solid elec-

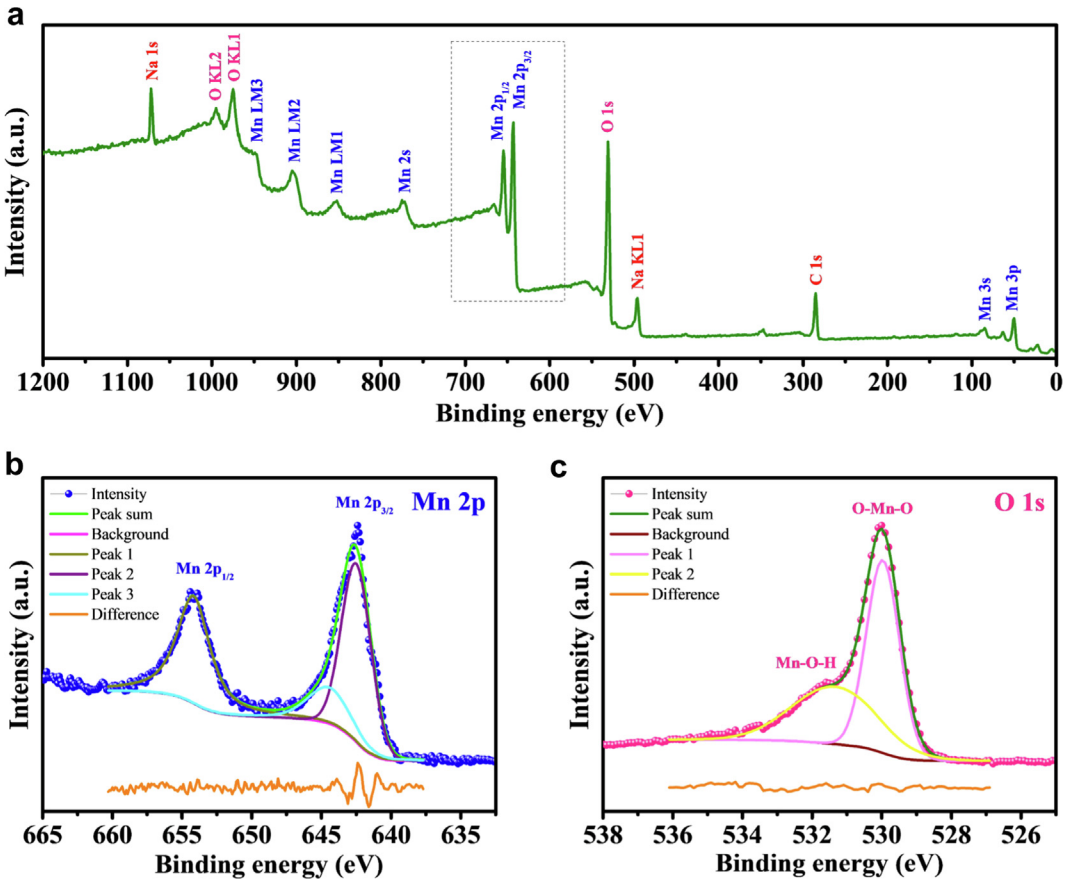

Fig. 2. (a) Survey XPS spectrum of as-prepared α-MnO_2. (b, c) XPS spectra deconvolution of core level spectra for Mn 2*p* and O 1*s*.

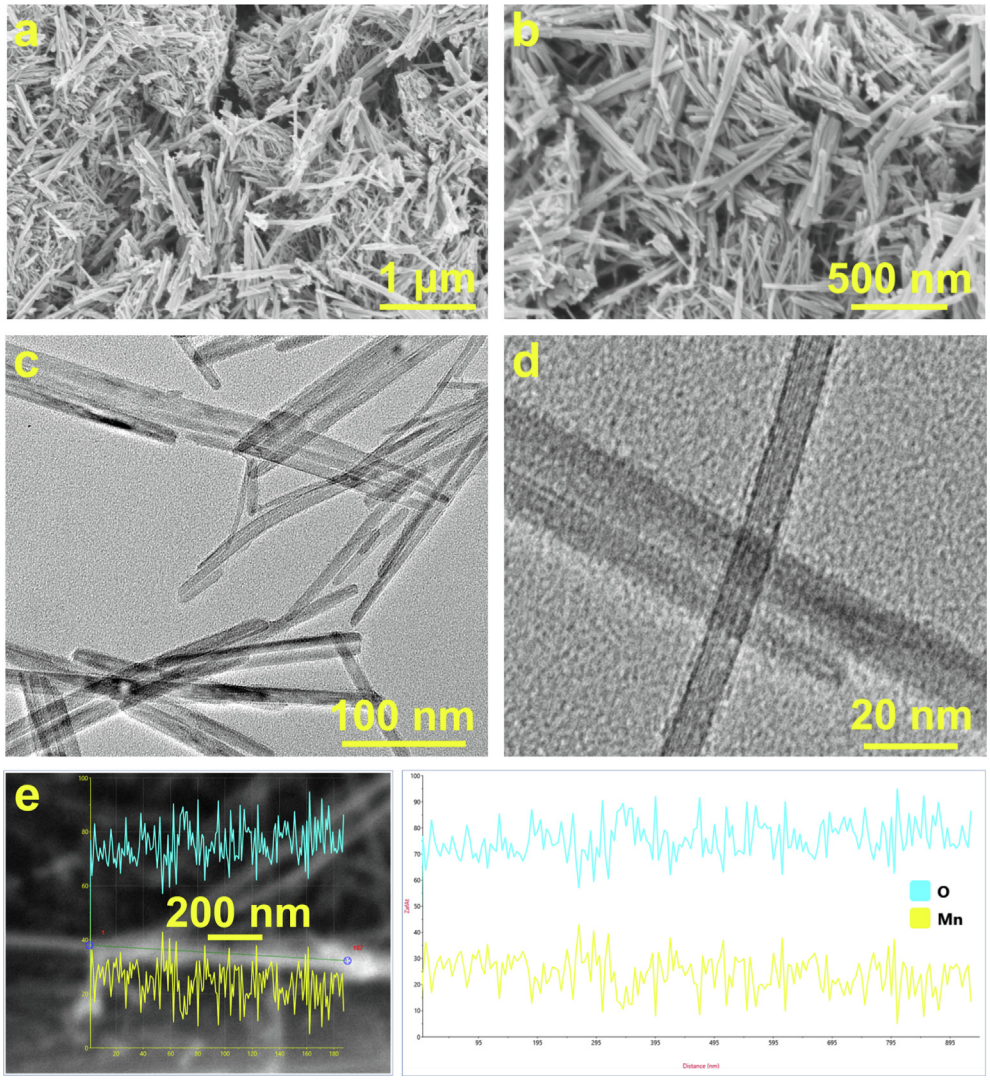

Fig. 3. (a, b) FESEM images and (c, d) HRTEM images of α-MnO_2. (e) EDS line scanning for the α-MnO_2; the yellow line refers to manganese (Mn), and the cyan line is assigned for oxygen (O).

trolyte interphase (SEI) [74–77]. The associated insertion/extraction reaction mechanism during the subsequent discharge/charge process for the MnO_2 electrode is described by the following equation [78,79]:

$$MnO_2 + xK^+ + xe^- \leftrightarrow K_xMnO_2 \quad (3)$$

In addition, a reasonable rate capability for KIBs was examined for the α-MnO_2 electrodes. Fig. 5 shows the rate performance of the α-MnO_2 electrode at various current densities ranging from C/20 to 5C. At 1.5–4 V, the α-MnO_2 electrode yields moderate reversible capacities up to C, but not able to achieve any capacity above C to 5C (Fig. 5**a, b**). A limited capacity is achieved when the current rate is again slowed down to C/20. Despite this, α-MnO_2 electrode executes better rate capability studies up to 5C in 1–4 V voltage range, addressing remarkable stability under all C-rates engaged in discharge/charge studies (Fig. 5**c, d**). K^+ have a lower Lewis acidity than Li^+, resulting in less correspondence with the Lewis-base in the electrolyte, leading in fast rate execution [80]. The open growth of α-MnO_2 would be advantageous for quick transport and diffusion of K^+ as well. Actually, the excellent rate performance appears to be attributable to MnO_2's unique nanorod-like structure, which is responsible for numerous electrochemical sites and the reduction of the K ion diffusion route while also limiting volume change. Because the polarization effect of K metal is more at high rates, the voltage loss under a high current at the electrode is negligible. Surprisingly, when current density increases, the discharge capacities decrease in case of two electrodes, owing to the sluggish rate of K^+ diffusion in the presence of high current density [81,82]. Their exceptional rate presentations without sacrificing high working voltage can be a valuable addition to any practical energy storage application.

Furthermore, Fig. 6 depicts the cycling of α-MnO_2 electrodes at C rate under predetermined voltage windows up to 100 cycles. The electrode at 1.5–4 V window reveals superior cycling dependability (Fig. 6**a**) and stable Coulombic efficiency than the 1–4 V window (Fig. 6**c**). Surprisingly, in the 1–4 V range, the capacity rapidly drops as far as feasible to zero. After the initial cycle, the Coulombic efficiency increases with cycle numbers and reaches 100 % after a few cycles as seen in both functional voltage windows for MnO_2 electrode. Significant difference has been found in terms of capacity retention between the electrodes. However, their charge/discharge profiles are similar in both cases (Fig. 6**b and d**). It implies that changing the voltage window might have an influence on α-MnO_2's electrochemical properties. **Fig. S2** shows the electrochemical impedance spectroscopy (EIS) evolutions of the cells before and after stability with equivalent circuit diagram. While

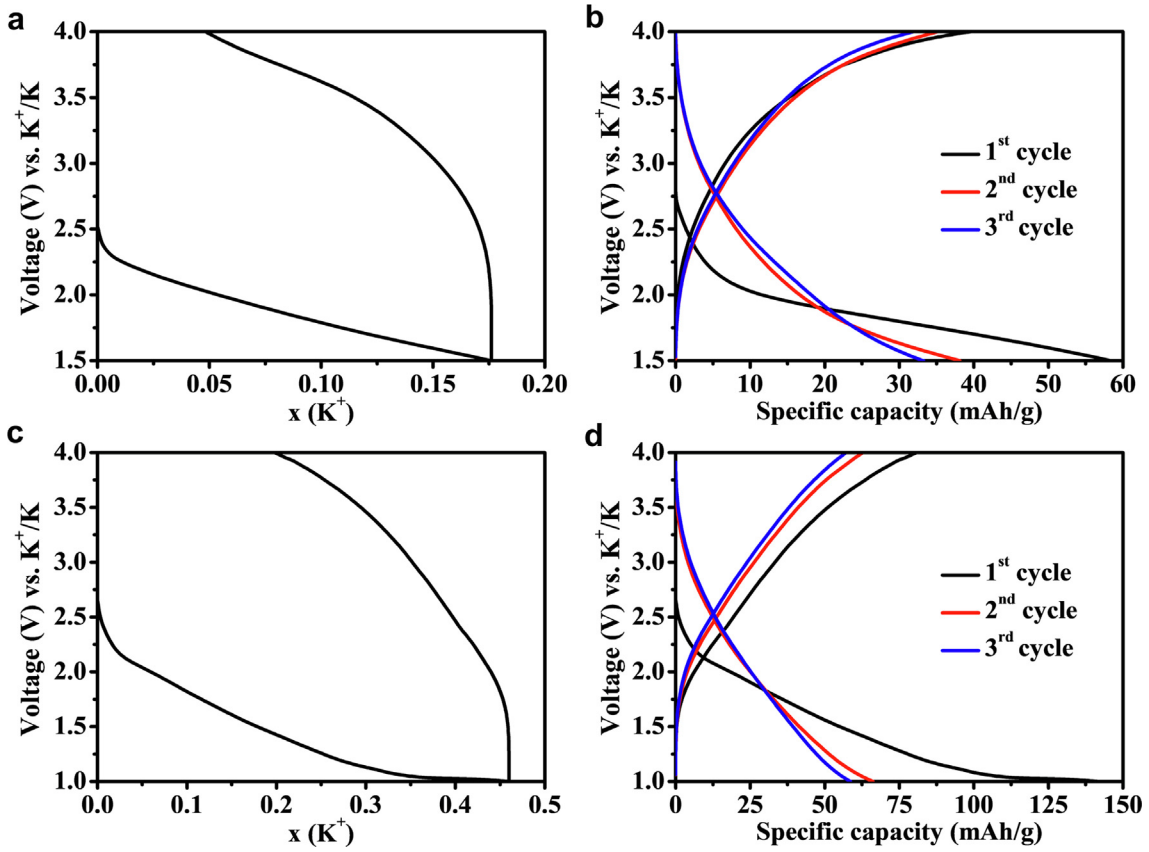

Fig. 4. Electrochemical charge/discharge curves per K^+ ion and cyclic voltage profiles in half potassium cells for α-MnO_2 in 1 M KPF_6 in EC:DEC at current rate of C/20 with a voltage window of (a and b) 1.5–4 V, and (c and d) 1–4 V.

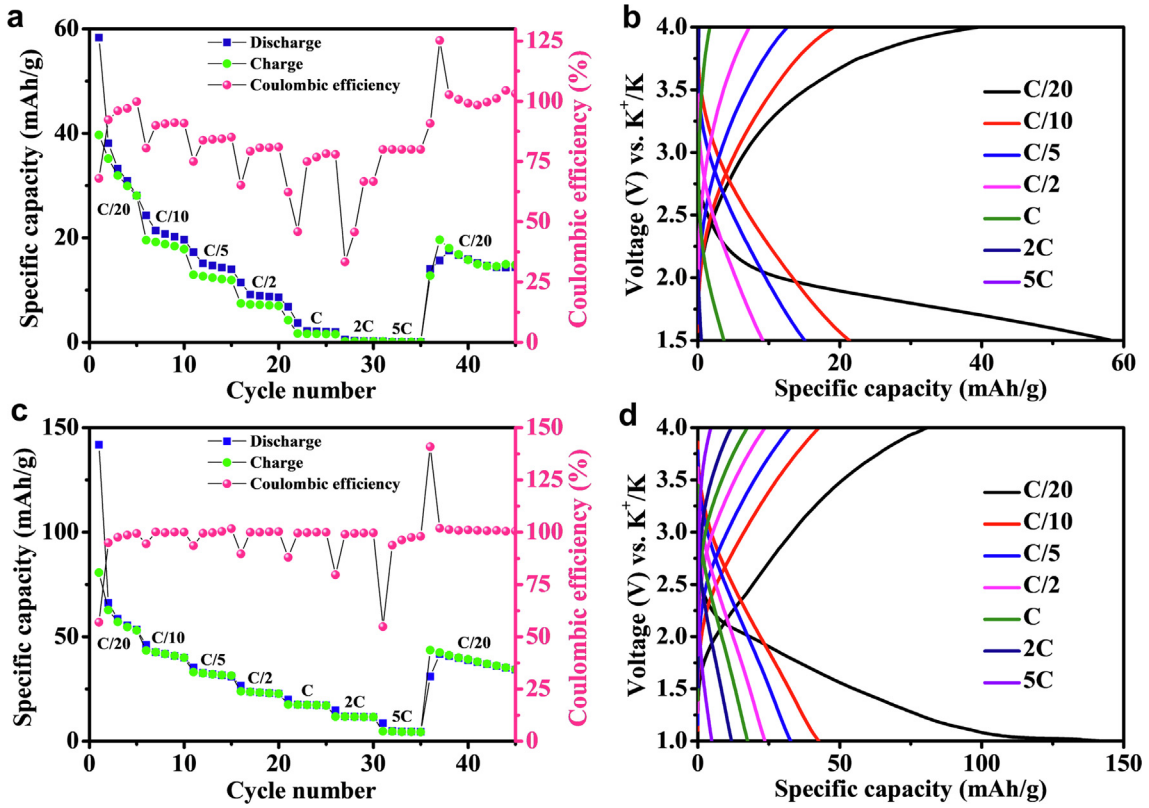

Fig. 5. Rate capability studies and charge–discharge curves α-MnO_2 at different C-rates between C/20 and 5C with a voltage window of (a and b) 1.5–4 V, and (c and d) 1–4 V.

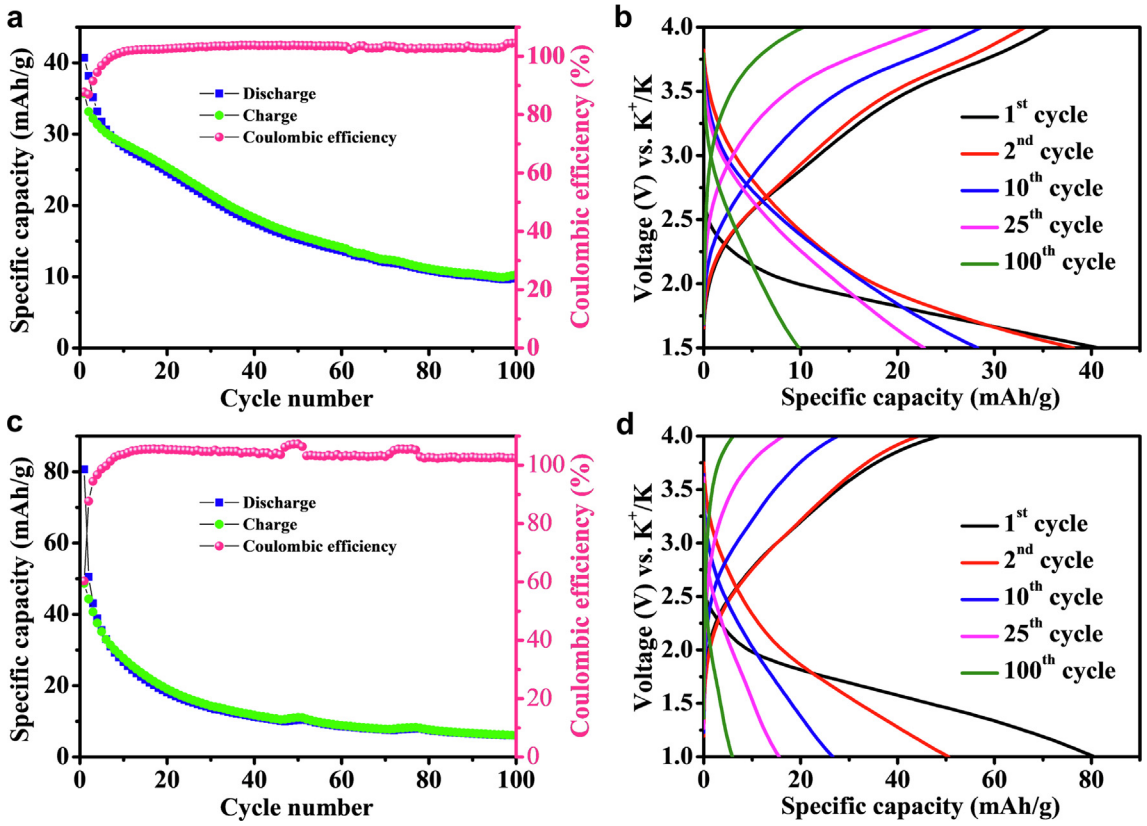

Fig. 6. The cycling performance and charge–discharge profiles of α-MnO_2 at C rate with a voltage window of (a and b) 1.5–4 V, and (c and d) 1–4 V.

the charge transfer resistance (R_{CT}) is depicted in the high frequency domain as a semicircular arc, the internal resistance (Rs) corresponds to an intersection point in the X-axis [83,84]. The double layer component inside pores and diffusion in the MnO_2 structure are coupled by the constant phase element (CPE) and Warburg resistance (W). The R_L component is linked to leakage resistance during electrochemical activities. It is evident that the Nyquist plot after stability test did not show any observable new semicircles, despite the semicircle's considerable increase with cycling. This reveals that cells cycled at high current undergo a significant rise in charge-transfer resistance and that the SEI layer formation is constrained as well [85].

3.3. Theoretical insights

The electronic structure and diffusion barrier of K^+ in the α-MnO_2 material are important factors that dictate the electrochemical performance. Considering these properties are not easy to determine experimentally, first-principles density functional theory (DFT) calculations were employed. The optimized structures of the pristine and K-intercalated α-MnO_2 with the corresponding charge density isosurface are shown in Fig. 7**a, b**. The lattice parameters are predicted at $a = b = 9.763$ Å, $c = 2.872$ Å (volume = 273.75 Å^3) for the pristine α-MnO_2 and at $_a = b = 9.71$ 9 Å and $c = 2.850$ Å (volume = 269.21 Å^3) for the K-intercalated α-MnO_2. This indicates that the incorporation of potassium contracts the unit cell volume of α-MnO_2 by 1.67 %. Bader population analyses reveal an increase in the atomic charge of the O atoms near to the Na ion in the one-dimensional tunnel, with the 4 nearest ones gaining extra charges of ~ 0.13 e^- (as indicated on Fig. 7**a, b**). The change of atomic charges before and after the insertion of K^+ can be attributed to the release on of one electron which redistributes to the nearest O atoms, increasing their negative charges. The reaction of K with α-MnO_2 (K + MnO_2 → $KMnO_2$) produced a voltage of 3.19 V, calculated from the relation $V = -\left(\frac{E(KMnO_2)-E(MnO_2)-E(K)}{N_{electrons}}\right)$, where $E(KMnO_2)$ is the energy of the K-intercalated α-MnO_2, $E(MnO_2)$ is the energy of the pristine α-MnO_2, E(K) is the energy K atom, and $N_{electrons}$ are the number of electrons transferred with the cation. Similar voltages have been reported for lithium (3.36 V) [86] and sodium (3.23–3.34 V) [87] intercalation in α-MnO_2. As shown in Fig. 7**c, d**, compared to the pristine material, the Fermi level K-intercalated α-MnO_2 is shifted to slightly above the edge conduction band (CB) edge, owing to the addition of an extra electron from the K^+ ion. An analysis of the projected density of states reveals that the valence band edge of both the pristine and K-incorporated α-MnO_2 is composed mainly of O-*p* states, whereas the conduction band edge is dominated by Mn-*d* states. Overall, the bandgap remained is not significantly affected by the incorporation of K^+ ion, predicted at 2.42 eV for the pristine α-MnO_2 and 2.30 eV for the K-α-MnO_2. This results are consistent with a previous theoretical investigation of Na incorporation in MnO_2 [87]. The reduction of the bandgap coupled with the shift of the Fermi level above the edge conduction band edge with K incorporation suggests improvement in the electrical conductivity of the K-α-MnO_2 compared to the pristine α-MnO_2. The diffusion pathway for K in α-MnO_2 and the corresponding calculated energy profile are shown in Fig. 7**e, f**. As shown in Fig. 7**e**, the K diffusion path in α-MnO_2 is investigated along the 1D tunnel within the 1 × 1 × 2 supercell with the K atom at the hollow site. The energy barrier for the migration of K^+ in the α-MnO_2 material is calculated at 0.31 eV, which is low enough to promote faster electrochemical kinetics for practical K-MnO_2 battery applications. The calculated migration energy barrier of K (0.31 eV), compared well with previous theoretical predictions for both Li ions and Na ions which are less than 0.3 eV [86]. The energy barrier for the

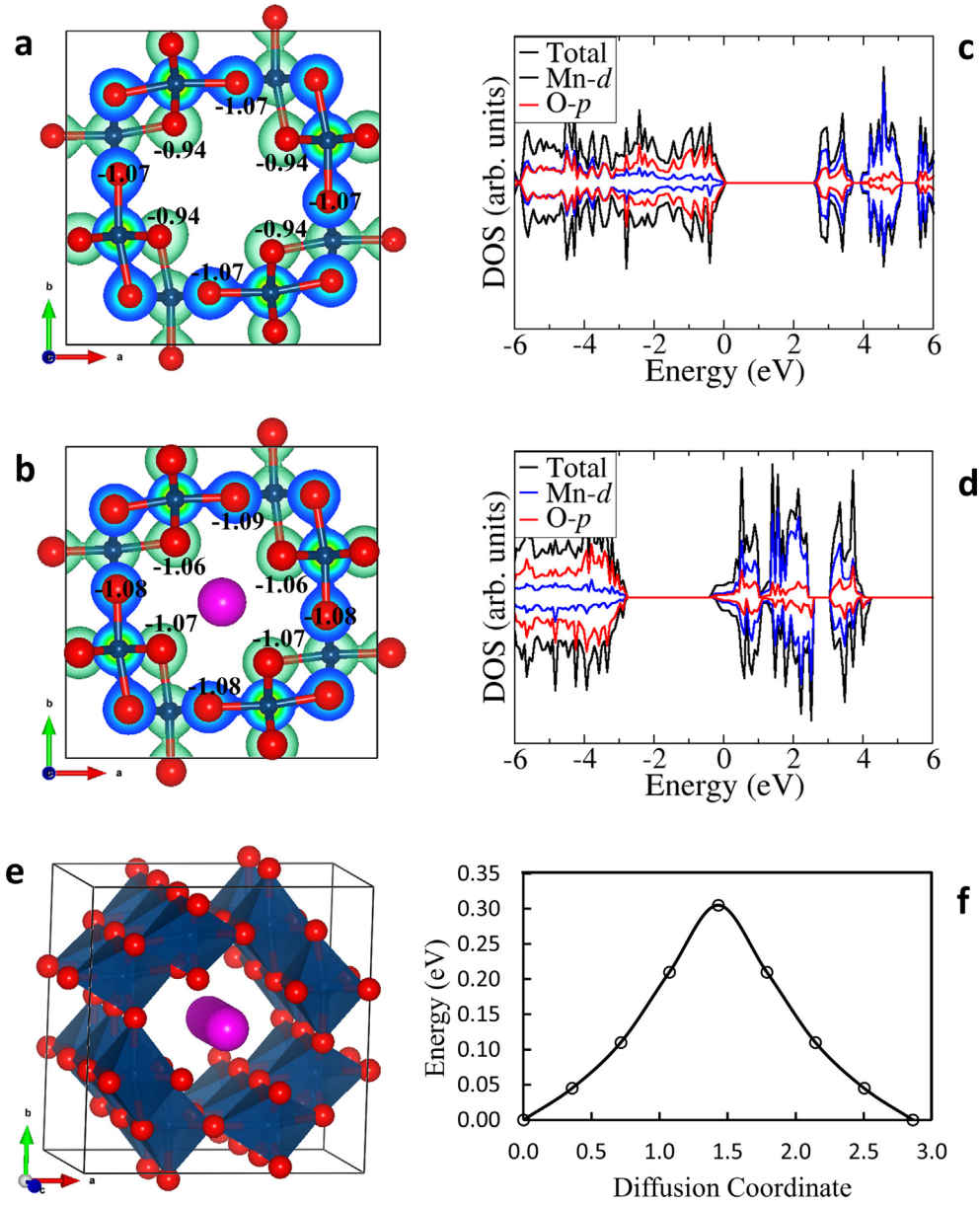

Fig. 7. Charge density distribution for (a) pristine and (b) K-intercalated α-MnO_2 and the corresponding partial density of states (c) and (d), respectively. (e) K ion diffusion pathway and (f) Energy profile of K ion diffusion path through α-MnO_2 1 × 1 × 2 supercell.

migration of Zn^{2+} in the α-MnO_2 structure was predicted to be 0.497 eV [88], whereas Ca through α-MnO_2 is predicted to encounter an energy barrier of 0.19 eV [89].

4. Conclusions

In conclusion, the nanorod morphology of α-MnO_2 is effectively structured using hydrothermal method followed by an annealing procedure. A good capacity (142 mAh/g as first discharge capacity), an excellent rate property (up to 5C), superb cycling execution (over 100 cycles) at room temperature are achieved for the α-MnO_2 cathode by optimizing the voltage window. The fabricated K-ion battery exhibits such electrochemical performance at high voltage window of 1–4 V in comparison with literature [90,91]. It is well acknowledged that remarkable improvement comes from the structural frameworks. The homogeneous structure provides more open framework associated with electrolyte–electrode interface, ensuring host ion insertion/extraction, and safeguarding the cathode from electrolyte interactions at high voltage. The redox reactions are aided by the α-MnO_2, which allows for quick charge movement in the structure as supported by DFT calculations. As a result, this research presents the strategy to fabricate future cathode materials with suitable proposal for exhibiting an excellent electrochemical behavior and extended cycle reliability in the framework of potassium ion batteries.

CRediT authorship contribution statement

Bidhan Pandit: Conceptualization, Data curation, Formal analysis, Writing – original draft, Writing – review & editing, Investigation, Methodology, Resources, Software, Validation, Visualization, Writing – review & editing, Supervision. **Sachin R. Rondiya:** Data curation, Software, Investigation, Methodology, Resources, Validation, Visualization, Writing – review & editing. **Shoyebmohamad F. Shaikh:** Data curation, Methodology, Investigation. **Mohd Ubaidullah:** Data curation, Methodology, Investigation. **Ricardo**

Amaral: Data curation, Software, Methodology, Investigation, Resources. **Nelson Y. Dzade:** Data curation, Software, Methodology, Investigation, Resources. **Emad S. Goda:** Data curation, Methodology, Investigation. **Abu ul Hassan Sarwar Rana:** Data curation, Methodology, Investigation. **Harjot Singh Gill:** Data curation, Methodology, Investigation. **Tokeer Ahmad:** Data curation, Methodology, Investigation.

Data availability

Data will be made available on request.

Declaration of Competing Interest

The authors declare that they have no known competing financial interests or personal relationships that could have appeared to influence the work reported in this paper.

Acknowledgements

The CONEX-Plus programme, supported by Universidad Carlos III de Madrid (UC3M) and the European Commission through the Marie Sklodowska Curie COFUND Action (Grant Agreement No 801538), is acknowledged by Bidhan Pandit. SRR acknowledges the support of the Department of Materials Engineering, Indian Institute of Science (IISc), Bengaluru, India. The authors are thankful to Abdolkhaled Mohammadi, Université de Montpellier (France) for his assistance with this project. The authors extend their sincere appreciation to the Researchers Supporting Project number (RSP-2021/370), King Saud University, Riyadh, Saudi Arabia for the financial support. SRR and NYD acknowledge the UK Engineering and Physical Sciences Research Council (EPSRC) for funding (Grant EP/S001395/1). RA and NYD acknowledge the support of the College of Earth and Minerals Sciences and the John and Willie Leone Family Department of Energy and Mineral Engineering of the Pennsylvania State University. Computer simulations for this work were performed on the Roar Supercomputer of the Pennsylvania State University. Authors acknowledge Universidad Carlos III de Madrid (Read & Publish Agreement CRUE-CSIC 2022) for funding the article processing charge (APC) to make this article open access.

Appendix A. Supplementary data

Supplementary data to this article can be found online at https://doi.org/10.1016/j.jcis.2022.11.070.

References

[1] R. Rajagopalan, Y. Tang, X. Ji, C. Jia, H. Wang, Advancements and Challenges in Potassium Ion Batteries: A Comprehensive Review, Adv. Funct. Mater. 30 (2020) 1909486, https://doi.org/10.1002/adfm.201909486.
[2] J. Liao, Y. Han, Z. Zhang, J. Xu, J. Li, X. Zhou, Recent Progress and Prospects of Layered Cathode Materials for Potassium-ion Batteries, Energy Environ. Mater. 4 (2021) 178–200, https://doi.org/10.1002/eem2.12166.
[3] C.S. Martínez-Cisneros, B. Pandit, C. Antonelli, J.Y. Sanchez, B. Levenfeld, A. Varez, Development of sodium hybrid quasi-solid electrolytes based on porous NASICON and ionic liquids, J. Eur. Ceram. Soc. 41 (2021) 7723–7733, https://doi.org/10.1016/j.jeurceramsoc.2021.08.001.
[4] P.U. Nzereogu, A.D. Omah, F.I. Ezema, E.I. Iwuoha, A.C. Nwanya, Anode materials for lithium-ion batteries: A review, Appl. Surf. Sci. Adv. 9 (2022), https://doi.org/10.1016/j.apsadv.2022.100233 100233.
[5] L.A. Román-Ramírez, J. Marco, Design of experiments applied to lithium-ion batteries: A literature review, Appl. Energy. 320 (2022), https://doi.org/10.1016/j.apenergy.2022.119305 119305.
[6] X. Bian, Y. Dong, D. Zhao, X. Ma, M. Qiu, J. Xu, L. Jiao, F. Cheng, N. Zhang, Microsized Antimony as a Stable Anode in Fluoroethylene Carbonate Containing Electrolytes for Rechargeable Lithium-/Sodium-Ion Batteries, ACS Appl. Mater. Interfaces. 12 (2020) 3554–3562, https://doi.org/10.1021/acsami.9b18006.
[7] C. Delmas, Sodium and Sodium-Ion Batteries: 50 Years of Research, Adv. Energy Mater. 8 (2018) 1703137, https://doi.org/10.1002/aenm.201703137.
[8] T. Perveen, M. Siddiq, N. Shahzad, R. Ihsan, A. Ahmad, M.I. Shahzad, Prospects in anode materials for sodium ion batteries - A review, Renew. Sustain. Energy Rev. 119 (2020), https://doi.org/10.1016/j.rser.2019.109549 109549.
[9] K. Chayambuka, G. Mulder, D.L. Danilov, P.H.L. Notten, Sodium-Ion Battery Materials and Electrochemical Properties Reviewed, Adv. Energy Mater. 8 (2018) 1800079, https://doi.org/10.1002/aenm.201800079.
[10] L. Li, Y. Zheng, S. Zhang, J. Yang, Z. Shao, Z. Guo, Recent progress on sodium ion batteries: Potential high-performance anodes, Energy Environ. Sci. 11 (2018) 2310–2340, https://doi.org/10.1039/c8ee01023d.
[11] J.M. Lee, G. Singh, W. Cha, S. Kim, J. Yi, S.J. Hwang, A. Vinu, Recent Advances in Developing Hybrid Materials for Sodium-Ion Battery Anodes, ACS Energy Lett. 5 (2020) 1939–1966, https://doi.org/10.1021/acsenergylett.0c00973.
[12] B. Pandit, M.T. Sougrati, B. Fraisse, L. Monconduit, Exploration of a Na3V2(PO4)3/C –Pb full cell Na-ion prototype, Nano Energy. 95 (2022), https://doi.org/10.1016/j.nanoen.2022.107010 107010.
[13] L. Yu, L. Shao, S. Wang, J. Guan, X. Shi, J. Cai, N. Tarasenko, Z. Sun, A low-cost NiSe2 derived from waste nickel foam as a high-performance anode for sodium ion batteries, Mater. Today Phys. 22 (2022), https://doi.org/10.1016/j.mtphys.2021.100593 100593.
[14] Z. Hu, Z. Zhu, F. Cheng, K. Zhang, J. Wang, C. Chen, J. Chen, Pyrite FeS2 for high-rate and long-life rechargeable sodium batteries, Energy Environ. Sci. 8 (2015) 1309–1316, https://doi.org/10.1039/c4ee03759f.
[15] S.K. Das, S. Mahapatra, H. Lahan, Aluminium-ion batteries: developments and challenges, J. Mater. Chem. A. 5 (2017) 6347–6367, https://doi.org/10.1039/c7ta00228a.
[16] D.u. Yuan, J. Zhao, W. Manalastas, S. Kumar, M. Srinivasan, Emerging rechargeable aqueous aluminum ion battery: Status, challenges, and outlooks, Nano, Mater. Sci. 2 (3) (2020) 248–263, https://doi.org/10.1016/j.nanoms.2019.11.001.
[17] Y. Ru, S. Zheng, H. Xue, H. Pang, Different positive electrode materials in organic and aqueous systems for aluminium ion batteries, J. Mater. Chem. A. 7 (2019) 14391–14418, https://doi.org/10.1039/c9ta01550g.
[18] Q. Guo, W. Zeng, S.L. Liu, Y.Q. Li, J.Y. Xu, J.X. Wang, Y. Wang, Recent developments on anode materials for magnesium-ion batteries: a review, Rare Met. 40 (2021) 290–308, https://doi.org/10.1007/s12598-020-01493-3.
[19] Z. Guo, S. Zhao, T. Li, D. Su, S. Guo, G. Wang, Recent Advances in Rechargeable Magnesium-Based Batteries for High-Efficiency Energy Storage, Adv. Energy Mater. 10 (2020) 1903591, https://doi.org/10.1002/aenm.201903591.
[20] F. Liu, T. Wang, X. Liu, L. Fan, Challenges and Recent Progress on Key Materials for Rechargeable Magnesium Batteries, Adv. Energy Mater. 11 (2021) 2000787, https://doi.org/10.1002/aenm.202000787.
[21] M. Asif, S. Kilian, M. Rashad, Uncovering electrochemistries of rechargeable magnesium-ion batteries at low and high temperatures, Energy Storage Mater. 42 (2021) 129–144, https://doi.org/10.1016/j.ensm.2021.07.031.
[22] C. Pei, F. Xiong, Y. Yin, Z. Liu, H. Tang, R. Sun, Q. An, L. Mai, Recent Progress and Challenges in the Optimization of Electrode Materials for Rechargeable Magnesium Batteries, Small. 17 (2021) 2004108, https://doi.org/10.1002/smll.202004108.
[23] X. Wu, D.P. Leonard, X. Ji, Emerging Non-Aqueous Potassium-Ion Batteries: Challenges and Opportunities, Chem. Mater. 29 (2017) 5031–5042, https://doi.org/10.1021/acs.chemmater.7b01764.
[24] X. Zou, P. Xiong, J. Zhao, J. Hu, Z. Liu, Y. Xu, Recent research progress in non-aqueous potassium-ion batteries, Phys. Chem. Chem. Phys. 19 (2017) 26495–26506, https://doi.org/10.1039/c7cp03852f.
[25] S. Zhao, Z. Guo, K. Yan, X. Guo, S. Wan, F. He, B. Sun, G. Wang, The Rise of Prussian Blue Analogs: Challenges and Opportunities for High-Performance Cathode Materials in Potassium-Ion Batteries, Small Struct. 2 (2021) 2000054, https://doi.org/10.1002/sstr.202000054.
[26] J. Ge, L. Fan, A.M. Rao, J. Zhou, B. Lu, Surface-substituted Prussian blue analogue cathode for sustainable potassium-ion batteries, Nat. Sustain. 2021 53. 5 (2021) 225–234. https://doi.org/10.1038/s41893-021-00810-7.
[27] Y. Hu, L. Fan, A.M. Rao, W. Yu, C. Zhuoma, Y. Feng, Z. Qin, J. Zhou, B. Lu, Cyclic-anion salt for high-voltage stable potassium-metal batteries, Natl. Sci. Rev. 9 (2022). https://doi.org/10.1093/nsr/nwac134.
[28] L. Fan, Y. Hu, A.M. Rao, J. Zhou, Z. Hou, C. Wang, B. Lu, Prospects of Electrode Materials and Electrolytes for Practical Potassium-Based Batteries, Small Methods. 5 (2021) 2101131, https://doi.org/10.1002/smtd.202101131.
[29] J. Li, Y. Hu, H. Xie, J. Peng, L. Fan, J. Zhou, B. Lu, Weak Cation-Solvent Interactions in Ether-Based Electrolytes Stabilizing Potassium-ion Batteries, Angew. Chemie. 134 (2022) e202208291, https://doi.org/10.1002/ange.202208291.
[30] J. Wu, Q. Zhang, S. Liu, J. Long, Z. Wu, W. Zhang, W.K. Pang, V. Sencadas, R. Song, W. Song, J. Mao, Z. Guo, Synergy of binders and electrolytes in enabling microsized alloy anodes for high performance potassium-ion batteries, Nano Energy. 77 (2020), https://doi.org/10.1016/j.nanoen.2020.105118 105118.
[31] J.C. Pramudita, D. Sehrawat, D. Goonetilleke, N. Sharma, An Initial Review of the Status of Electrode Materials for Potassium-Ion Batteries, Adv. Energy Mater. 7 (2017) 1602911, https://doi.org/10.1002/aenm.201602911.
[32] M. Sha, L. Liu, H. Zhao, Y. Lei, Review on Recent Advances of Cathode Materials for Potassium-ion Batteries, Energy Environ. Mater. 3 (2020) 56–66, https://doi.org/10.1002/eem2.12060.
[33] W. Zhang, J. Yin, W. Wang, Z. Bayhan, H.N. Alshareef, Status of rechargeable potassium batteries, Nano Energy. 83 (2021), https://doi.org/10.1016/j.nanoen.2021.105792 105792.

[34] S. Liu, L. Kang, S.C. Jun, Challenges and Strategies toward Cathode Materials for Rechargeable Potassium-Ion Batteries, Adv. Mater. 33 (2021) 2004689, https://doi.org/10.1002/adma.202004689.
[35] X. Huang, J. Sun, L. Wang, X. Tong, S.X. Dou, Z.M. Wang, Advanced High-Performance Potassium-Chalcogen (S, Se, Te) Batteries, Small. 17 (2021) 2004369, https://doi.org/10.1002/smll.202004369.
[36] Y. Wang, D. Liu, M. Sun, J. Liu, Recent progress in electrode materials for aqueous sodium and potassium ion batteries, Mater. Chem. Front. 5 (2021) 7384–7402, https://doi.org/10.1039/d1qm01011e.
[37] Z. Liu, H. Su, Y. Yang, T. Wu, S. Sun, H. Yu, Advances and perspectives on transitional metal layered oxides for potassium-ion battery, Energy Storage Mater. 34 (2021) 211–228, https://doi.org/10.1016/j.ensm.2020.09.010.
[38] B. Wang, E.H. Ang, Y. Yang, Y. Zhang, M. Ye, Q. Liu, C.C. Li, Post-Lithium-Ion Battery Era: Recent Advances in Rechargeable Potassium-Ion Batteries, Chem. - A Eur. J. 27 (2021) 512–536, https://doi.org/10.1002/chem.202001811.
[39] Y. Matsuda, H. Nakashima, M. Morita, Y. Takasu, Behavior of Some Ions in Mixed Organic Electrolytes of High Energy Density Batteries, J. Electrochem. Soc. 128 (12) (1981) 2552–2556, https://doi.org/10.1149/1.2127289.
[40] M. Moshkovich, Y. Gofer, D. Aurbach, Investigation of the Electrochemical Windows of Aprotic Alkali Metal (Li, Na, K) Salt Solutions, J. Electrochem. Soc. 148 (2001) E155, https://doi.org/10.1149/1.1357316.
[41] Y. Xu, C. Zhang, M. Zhou, Q. Fu, C. Zhao, M. Wu, Y. Lei, Highly nitrogen doped carbon nanofibers with superior rate capability and cyclability for potassium ion batteries, Nat. Commun. 9 (2018) 1720, https://doi.org/10.1038/s41467-018-04190-z.
[42] I. Sultana, M.M. Rahman, T. Ramireddy, Y. Chen, A.M. Glushenkov, Correction: High capacity potassium-ion battery anodes based on black phosphorus, J. Mater. Chem. A. 7 (2019) 2421–2421. https://doi.org/10.1039/C9TA90016K.
[43] I. Sultana, T. Ramireddy, M.M. Rahman, Y. Chen, A.M. Glushenkov, Tin-based composite anodes for potassium-ion batteries, Chem. Commun. 52 (2016) 9279–9282, https://doi.org/10.1039/c6cc03649j.
[44] W.D. McCulloch, X. Ren, M. Yu, Z. Huang, Y. Wu, Potassium-Ion Oxygen Battery Based on a High Capacity Antimony Anode, ACS Appl. Mater. Interfaces. 7 (2015) 26158–26166, https://doi.org/10.1021/acsami.5b08037.
[45] J. Huang, X. Lin, H. Tan, B. Zhang, Bismuth Microparticles as Advanced Anodes for Potassium-Ion Battery, Adv. Energy Mater. 8 (2018) 1703496, https://doi.org/10.1002/aenm.201703496.
[46] L. Xue, H. Gao, W. Zhou, S. Xin, K. Park, Y. Li, J.B. Goodenough, Liquid K-Na Alloy Anode Enables Dendrite-Free Potassium Batteries, Adv. Mater. 28 (2016) 9608–9612, https://doi.org/10.1002/adma.201602633.
[47] W. Zhang, W.K. Pang, V. Sencadas, Z. Guo, Understanding High-Energy-Density Sn4P3 Anodes for Potassium-Ion Batteries, Joule. 2 (2018) 1534–1547, https://doi.org/10.1016/j.joule.2018.04.022.
[48] Q. Deng, J. Pei, C. Fan, J. Ma, B. Cao, C. Li, Y. Jin, L. Wang, J. Li, Potassium salts of para-aromatic dicarboxylates as the highly efficient organic anodes for low-cost K-ion batteries, Nano Energy. 33 (2017) 350–355, https://doi.org/10.1016/j.nanoen.2017.01.016.
[49] P. Lian, Y. Dong, Z.-S. Wu, S. Zheng, X. Wang, Sen Wang, C. Sun, J. Qin, X. Shi, X. Bao, Alkalized Ti3C2 MXene nanoribbons with expanded interlayer spacing for high-capacity sodium and potassium ion batteries, Nano Energy. 40 (2017) 1–8, https://doi.org/10.1016/j.nanoen.2017.08.002.
[50] I. Sultana, M.M. Rahman, S. Mateti, V.G. Ahmadabadi, A.M. Glushenkov, Y. Chen, K-ion and Na-ion storage performances of Co3O4-Fe2O3 nanoparticle-decorated super P carbon black prepared by a ball milling process, Nanoscale. 9 (2017) 3646–3654, https://doi.org/10.1039/c6nr09613a.
[51] H. Gao, T. Zhou, Y. Zheng, Q. Zhang, Y. Liu, J. Chen, H. Liu, Z. Guo, CoS Quantum Dot Nanoclusters for High-Energy Potassium-Ion Batteries, Adv. Funct. Mater. 27 (2017) 1702634, https://doi.org/10.1002/adfm.201702634.
[52] Y. Yang, S. Song, F. Jiang, J. Zhou, W. Sun, Short process for regenerating Mn-rich cathode material with high voltage from mixed-type spent cathode materials via a facile approach, J. Clean. Prod. 186 (2018) 123–130, https://doi.org/10.1016/j.jclepro.2018.03.147.
[53] C. Zhan, X. Qiu, J. Lu, K. Amine, Tuning the Mn Deposition on the Anode to Improve the Cycle Performance of the Mn-Based Lithium Ion Battery, Adv. Mater. Interfaces. 3 (2016) 1500856, https://doi.org/10.1002/admi.201500856.
[54] S. Chong, Y. Wu, Y. Chen, S. Guo, Z. Tai, C. Shu, Q. Tan, J. Sun, Y. Liu, Mn-based layered oxide microspheres assembled by ultrathin nanosheets as cathode material for potassium-ion batteries, Electrochim. Acta. 293 (2019) 299–306, https://doi.org/10.1016/j.electacta.2018.10.009.
[55] M. Huang, F. Li, F. Dong, Y.X. Zhang, L.L. Zhang, MnO2-based nanostructures for high-performance supercapacitors, J. Mater. Chem. A. 3 (2015) 21380–21423, https://doi.org/10.1039/c5ta05523g.
[56] H. Liu, Z. Hu, L. Tian, Y. Su, H. Ruan, L. Zhang, R. Hu, Reduced graphene oxide anchored with δ-MnO2 nanoscrolls as anode materials for enhanced Li-ion storage, Ceram. Int. 42 (2016) 13519–13524, https://doi.org/10.1016/j.ceramint.2016.05.144.
[57] A. Baral, L. Satish, G. Zhang, S. Ju, M.K. Ghosh, A Review of Recent Progress on Nano MnO2: Synthesis, Surface Modification and Applications, J. Inorg. Organomet. Polym. Mater. 31 (2021) 899–922, https://doi.org/10.1007/s10904-020-01823-z.
[58] B. Pandit, E.S. Goda, M.H. Abu Elella, A. ur Rehman, S. Eun Hong, S.R. Rondiya, P. Barkataki, S.F. Shaikh, A.M. Al-Enizi, S.M. El-Bahy, K. Ro Yoon, One-pot hydrothermal preparation of hierarchical manganese oxide nanorods for high-performance symmetric supercapacitors, J. Energy Chem. 65 (2022) 116–126, https://doi.org/10.1016/j.jechem.2021.05.028.
[59] M. Sundararajan, A. Subramani, M. Ubaidullah, S.F. Shaikh, B. Pandit, S.K. Jesudoss, M. Kamalakannan, S. Yuvaraj, P.S. Subudhi, C.S. Dash, Synthesis, Characterization and In Vitro Cytotoxic Effects of Cu:Co3O4 Nanoparticles Via Microwave Combustion Method, J. Clust. Sci. 33 (2022) 1821–1830, https://doi.org/10.1007/s10876-022-02239-0.
[60] M. Shkir, A. Ben Gouider Trabelsi, F.H. Alkallas, S. AlFaify, B. Pandit, M. Ubaidullah, Improved Optoelectronic Properties of Nanostructured Eu Doped Bi2S3 Thin Films for the Detection of UV Light, Crystals. 12 (2022) 1329, https://doi.org/10.3390/cryst12101329.
[61] T. Gao, H. Fjellvåg, P. Norby, A comparison study on Raman scattering properties of α- and β-MnO2, Anal. Chim. Acta. 648 (2009) 235–239, https://doi.org/10.1016/j.aca.2009.06.059.
[62] S. Cheng, L. Yang, D. Chen, X.u. Ji, Z.-J. Jiang, D. Ding, M. Liu, Phase evolution of an alpha MnO2-based electrode for pseudo-capacitors probed by in operando Raman spectroscopy, Nano Energy. 9 (2014) 161–167, https://doi.org/10.1016/j.nanoen.2014.07.008.
[63] M. Du, Y. Bu, Y. Zhou, Y. Zhao, S. Wang, H. Xu, Peptide-templated synthesis of branched MnO 2 nanowires with improved electrochemical performances, RSC Adv. 7 (2017) 12711–12718, https://doi.org/10.1039/C7RA00829E.
[64] D. Barreca, F. Gri, A. Gasparotto, G. Carraro, L. Bigiani, T. Altantzis, B. Žener, U. Lavrenčič Štangar, B. Alessi, D.B. Padmanaban, D. Mariotti, C. Maccato, Multi-functional MnO2 nanomaterials for photo-activated applications by a plasma-assisted fabrication route, Nanoscale. 11 (2018) 98–108, https://doi.org/10.1039/C8NR06468G.
[65] R.A. Davoglio, G. Cabello, J.F. Marco, S.R. Biaggio, Synthesis and characterization of α-MnO2 nanoneedles for electrochemical supercapacitors, Electrochim. Acta. 261 (2018) 428–435, https://doi.org/10.1016/j.electacta.2017.12.118.
[66] E. Miniach, A. Śliwak, A. Moyseowicz, L. Fernández-Garcia, Z. González, M. Granda, R. Menendez, G. Gryglewicz, MnO2/thermally reduced graphene oxide composites for high-voltage asymmetric supercapacitors, Electrochim. Acta. 240 (2017) 53–62, https://doi.org/10.1016/j.electacta.2017.04.056.
[67] D. Guo, S. Dou, X. Li, J. Xu, S. Wang, L. Lai, H.K. Liu, J. Ma, S.X. Dou, Hierarchical MnO2/rGO hybrid nanosheets as an efficient electrocatalyst for the oxygen reduction reaction, Int. J. Hydrogen Energy. 41 (2016) 5260–5268, https://doi.org/10.1016/j.ijhydene.2016.01.070.
[68] Z.-S. Wu, W. Ren, D.-W. Wang, F. Li, B. Liu, H.-M. Cheng, High-Energy MnO 2 Nanowire/Graphene and Graphene Asymmetric Electrochemical Capacitors, ACS Nano. 4 (2010) 5835–5842, https://doi.org/10.1021/nn101754k.
[69] K.-H. Ye, Z.-Q. Liu, C.-W. Xu, N. Li, Y.-B. Chen, Y.-Z. Su, MnO2/reduced graphene oxide composite as high-performance electrode for flexible supercapacitors, Inorg. Chem. Commun. 30 (2013) 1–4, https://doi.org/10.1016/j.inoche.2012.12.035.
[70] C. Li, Z. Yu, H. Liu, L. Kong, Dandelion-like α-MnO2 hollow spheres with superior catalytic performance for Li-O2 batteries by a facile in situ pyrolysis, J. Mater. Sci. 53 (2018) 14525–14535, https://doi.org/10.1007/s10853-018-2629-1.
[71] B. Pandit, S.R. Rondiya, R.W. Cross, N.Y. Dzade, B.R. Sankapal, Vanadium telluride nanoparticles on MWCNTs prepared by successive ionic layer adsorption and reaction for solid-state supercapacitor, Chem. Eng. J. 429 (2022), https://doi.org/10.1016/j.cej.2021.132505 132505.
[72] B. Pandit, B.R. Sankapal, Cerium Selenide Nanopebble/Multiwalled Carbon Nanotube Composite Electrodes for Solid-State Symmetric Supercapacitors, ACS Appl. Nano Mater. 5 (2022) 3007–3017, https://doi.org/10.1021/acsanm.2c00374.
[73] B. Pandit, B.R. Sankapal, Highly conductive energy efficient electroless anchored silver nanoparticles on MWCNTs as a supercapacitive electrode, New J. Chem. 41 (2017) 10808–10814, https://doi.org/10.1039/c7nj01792h.
[74] X. Dong, L. Li, C. Zhao, H.K. Liu, Z. Guo, Controllable synthesis of RGO/FexOy nanocomposites as high-performance anode materials for lithium ion batteries, J. Mater. Chem. A. 2 (2014) 9844–9850, https://doi.org/10.1039/C4TA01804D.
[75] B. Pandit, E.S. Goda, M. Ubaidullah, S.F. Shaikh, U.T. Nakate, A.P. Khedulkar, A.u. H.S. Rana, D. Kumar, R.-a. Doong, Hexagonal δ-MnO2 nanoplates as efficient cathode material for potassium-ion batteries, Ceram. Int. 48 (19) (2022) 28856–28863, https://doi.org/10.1016/j.ceramint.2022.03.279.
[76] B. Pandit, B. Fraisse, L. Stievano, L. Monconduit, M.T. Sougrati, Carbon-coated FePO4 nanoparticles as stable cathode for Na-ion batteries: A promising full cell with a Na15Pb4 anode, Electrochim. Acta. 409 (2022), https://doi.org/10.1016/j.electacta.2022.139997 139997.
[77] M.A. Jamil, G. Ali, K.I. Khan, F. Jan Iftikhar, S. Zaman, S.F. Shaikh, B. Pandit, Q. Wali, S.A. Patil, Highly efficient tin fluoride nanocomposite with conductive carbon as a high performance anode for Li-ion batteries, J. Alloys Compd. 900 (2022), https://doi.org/10.1016/j.jallcom.2021.163447 163447.
[78] X.N. Tang, S.K. Zhu, J. Ning, X.F. Yang, M.Y. Hu, J.J. Shao, Charge storage mechanisms of manganese dioxide-based supercapacitors: A review, Xinxing Tan Cailiao/New Carbon Mater. 36 (2021) 702–710, https://doi.org/10.1016/S1872-5805(21)60082-3.
[79] S. Deng, L. Wang, T. Hou, Y. Li, Two-Dimensional MnO2 as a Better Cathode Material for Lithium Ion Batteries, J. Phys. Chem. C. 119 (2015) 28783–28788, https://doi.org/10.1021/acs.jpcc.5b10354.
[80] K. Chihara, A. Katogi, K. Kubota, S. Komaba, KVPO4F and KVOPO4 toward 4 volt-class potassium-ion batteries, Chem. Commun. 53 (2017) 5208–5211, https://doi.org/10.1039/c6cc10280h.
[81] X. Dai, M. Zhang, T. Li, X. Cui, Y. Shi, X. Zhu, P. Wangyang, D. Yang, J. Li, Effect of current on electrodeposited MnO2 as supercapacitor and lithium-ion battery

electrode, Vacuum. 195 (2022), https://doi.org/10.1016/j.vacuum.2021.110692 110692.
[82] N. Zhao, S. Wu, C. He, Z. Wang, C. Shi, E. Liu, J. Li, One-pot synthesis of uniform Fe3O4 nanocrystals encapsulated in interconnected carbon nanospheres for superior lithium storage capability, Carbon N. Y. 57 (2013) 130–138, https://doi.org/10.1016/j.carbon.2013.01.056.
[83] W. Zong, H. Guo, Y. Ouyang, L. Mo, C. Zhou, G. Chao, J. Hofkens, Y. Xu, W. Wang, Y. Miao, G. He, I.P. Parkin, F. Lai, T. Liu, Topochemistry-Driven Synthesis of Transition-Metal Selenides with Weakened Van Der Waals Force to Enable 3D-Printed Na-Ion Hybrid Capacitors, Adv. Funct. Mater. 32 (2022) 2110016, https://doi.org/10.1002/adfm.202110016.
[84] V.D. Dang, T. Annadurai, A.P. Khedulkar, J.-Y. Lin, J. Adorna, W.-J. Yu, B. Pandit, T.V. Huynh, R.-A. Doong, S-scheme N-doped carbon dots anchored g-C3N4/Fe2O3 shell/core composite for photoelectrocatalytic trimethoprim degradation and water splitting, Appl. Catal. B Environ. 320 (2023), https://doi.org/10.1016/j.apcatb.2022.121928 121928.
[85] Y. Shen, S. Birgisson, B.B. Iversen, A,, P2-Na x Co 0.7 Mn 0.3 O 2 (x ≈ 1.0) cathode material for Na-ion batteries with superior rate and cycle capability, J. Mater. Chem. A. 4 (2016) 12281–12288, https://doi.org/10.1039/C6TA03630A.
[86] D.A. Tompsett, M.S. Islam, Electrochemistry of Hollandite α-MnO 2: Li-Ion and Na-Ion Insertion and Li 2 O Incorporation, Chem. Mater. 25 (2013) 2515–2526, https://doi.org/10.1021/cm400864n.
[87] B. Pandit, S.R. Rondiya, N.Y. Dzade, S.F. Shaikh, N. Kumar, E.S. Goda, A.A. Al-Kahtani, R.S. Mane, S. Mathur, R.R. Salunkhe, High Stability and Long Cycle Life of Rechargeable Sodium-Ion Battery Using Manganese Oxide Cathode: A Combined Density Functional Theory (DFT) and Experimental Study, ACS Appl. Mater. Interfaces. 13 (2021) 11433–11441, https://doi.org/10.1021/acsami.0c21081.
[88] H. Shen, B. Liu, Z. Nie, Z. Li, S. Jin, Y. Huang, H. Zhou, A comparison study of MnO 2 and Mn 2 O 3 as zinc-ion battery cathodes: an experimental and computational investigation, RSC Adv. 11 (2021) 14408–14414, https://doi.org/10.1039/D1RA00346A.
[89] T.R. Juran, J. Young, M. Smeu, Density Functional Theory Modeling of MnO 2 Polymorphs as Cathodes for Multivalent Ion Batteries, J. Phys. Chem. C. 122 (2018) 8788–8795, https://doi.org/10.1021/acs.jpcc.8b00918.
[90] S. Chong, Y. Wu, C. Liu, Y. Chen, S. Guo, Y. Liu, G. Cao, Cryptomelane-type MnO2/carbon nanotube hybrids as bifunctional electrode material for high capacity potassium-ion full batteries, Nano Energy. 54 (2018) 106–115, https://doi.org/10.1016/j.nanoen.2018.09.072.
[91] Z. Wang, X. Yan, F. Wang, T. Xiong, M.-S. Balogun, H. Zhou, J. Deng, Reduced graphene oxide thin layer induced lattice distortion in high crystalline MnO2 nanowires for high-performance sodium- and potassium-ion batteries and capacitors, Carbon N. Y. 174 (2021) 556–566, https://doi.org/10.1016/j.carbon.2020.12.071.

Bidhan Pandit is now a Marie Curie CONEX-Plus researcher at Universidad Carlos III de Madrid (UC3M), Madrid, Spain. He received his Ph.D. degree (2019) in Physics from Visvesvaraya National Institute of Technology (India) and joined as CNRS Postdoctoral Research Fellow at the Institut Charles Gerhardt Montpellier (ICGM), Université de Montpellier (France). His previous scientific interests focus on the synthesis of nanostructures and fabrication of flexible devices for supercapacitor applications. His current research focus includes the synthesis of cathode materials for lithium, sodium and potassium-ion batteries, as well as the *in situ*/*operando* X-ray based characterizations for the understanding of battery mechanisms.